

СООБЩЕНИЯ
ОБЪЕДИНЕННОГО
ИНСТИТУТА
ЯДЕРНЫХ
ИССЛЕДОВАНИЙ

Дубна

99-31 .

E13-99-31

TRACK CALORIMETER (TCAL) OF
ALPHA MAGNETIC SPECTROMETER (AMS)
(A Particle Physics Experiment
on the International Space Station Alpha)*

Dubna-Kiev-Kharkov-Tbilisi Collaboration

*Proposal submitted to JINR Programme Advisory Committee for
Particle Physics, April 1999

1999

Трековый калориметр (TCAL) для Alpha магнитного спектрометра (AMS)**(эксперимент на международной космической станции Alpha)**

На основе результатов моделирования и методических работ представлен проект ОИЯИ — дооснастить AMS-детектор трековым сцинтилляционным калориметром (TCAL) с тонкой пространственной грануляцией. Ориентировочная стоимость проекта 1 млн. долларов США. Такой калориметр позволит существенно увеличить потенциал AMS в изучении проблем возникновения и эволюции Вселенной: космической антиматерии, темной материи, а также более точного измерения ядерного состава космического излучения.

Работа выполнена в Лаборатории ядерных проблем ОИЯИ.

Сообщение Объединенного института ядерных исследований. Дубна, 1999

Anosov V. et al.

E13-99-31

**Track Calorimeter (TCAL) of Alpha Magnetic Spectrometer (AMS)
(A Particle Physics Experiment on the International Space
Station Alpha)**

Based on the simulation and R&D results the JINR project — to supplement AMS with a finely granulated scintillator track calorimeter (TCAL) — is discussed. The project cost is about 1 million USD. TCAL would essentially increase the AMS potential in the studies of antimatter, matter and missing matter in the experiments in outer space.

The investigation has been performed at the Laboratory of Nuclear Problems, JINR.

V. Anosov, S. Baranov, V. Bednyakov, V. Boreiko, G. Chelkov, D. Dedovitch, A. Dolbilov, Yu. Gornushkin, V. Grebenyuk, M. Ignatenko, A. Kalinin, N. Khovanski, Z. Krumstein, I. Minashvili, M. Nikolenko, A. Nozdrin, A. Olshevski, A. Sadovski, Z. Salukvadze, Yu. Sedykh, A. Selivanov, V. Shigaev, L. Tkachev, V. Tokmenin, N. Zhuravlev

Joint Institute for Nuclear Research, Dubna, Russia

I. Chupin, I. Seleznev, G. Vershinin

«Raduga» Machine-Building Design Bureau, Dubna, Russia

E. Mazepa

«Contact» Computer Communication Organization, Dubna, Russia

V. Borshchov, S. Kuprich, E. Listratenko

Scientific and Technological Research Institute of Instrument Engineering, Kharkov, Ukraine

V. Senchishin

Institute of Monocrystals, Kharkov, Ukraine

S. Mashkevich, O. Pavlenko, Yu. Shtanov, G. Zinovjev

Bogolubov Institute for Theoretical Physics, Kiev, Ukraine

I. Mestvirishvili

1 Introduction

To address fundamental questions in astroparticle physics, two state-of-the-art detectors based on high grade permanent magnets, the Alpha Magnetic Spectrometer (AMS) [1] and PAMELA [2] are being prepared for launching to the Earth orbit at the beginning of the next century. The AMS has been approved by NASA to operate on the International Space Station Alpha (ISSA), and a precursor test flight was fulfilled in June 1998.

The physics objectives of AMS are:

- Search for antimatter ($\bar{\text{He}}$ and $\bar{\text{C}}$) in space with a sensitivity 10^4 to 10^5 times better than the current limits.
- Search for dark matter by high statistics precision measurements of \bar{p} , e^+ and γ spectra.
- Astrophysical studies by high statistics measurements of D, ^3He , B, C, ^9Be and ^{10}Be spectra.

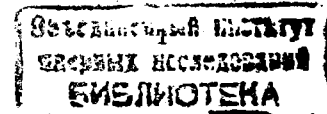
In the existing AMS design there is no electromagnetic or hadronic calorimeter which are essential parts of modern high energy physics apparatus.

Here the JINR project to add a high granular electromagnetic track calorimeter (TCAL) to the AMS detector is presented. But first the current state of fundamental research problems is briefly outlined.

1.1 Antimatter

By the word *antimatter* one means a matter-like material constituted by antiparticles, that is the counterparts of ordinary particles with the same properties but with inverted characteristic charges of fundamental interactions [3]. The existence of antimatter is an important result of quantum field theory, which implies that the creation of matter must occur simultaneously with the creation of antimatter. These fundamental results concerning matter at its microscopic level, when they are applied to standard cosmology based on the hot Big Bang singularity and on the subsequent expansion of the Universe, suggest cosmological models where the particle content of the Universe should be identical to its antiparticle content. Such symmetric cosmological models were conceived in spite of the fact that our common experience on the Earth and speculation concerning the nearby astronomical objects do not correspond to this scheme.

The consequent formulation by Sakharov [4] of his famous three conditions of baryogenesis (a mechanism of evolution of a baryon-symmetric Universe to an asymmetric one) allows us to conceive a matter-dominated Universe and the construction of asymmetric cosmological theories. These conditions are: (1) The number of baryons is not conserved (i.e. baryon-nonconserving interactions); (2) Charge conjugation symmetry (C) and the product of charge conjugation symmetry and parity (CP) both are not exact symmetries; (3) Baryogenesis could have occurred only during a period when the Universe was not in thermal equilibrium. Otherwise the balance between matter and antimatter would be maintained since the mass is the same for a particle and



an antiparticle (via the CPT theorem, which is believed to be true for all acceptable theories of particle physics)¹.

No data from particle accelerator experiments or proton decay experiments has provided evidence for baryon number violation so far. However, since there is no symmetry which guarantees baryonic charge conservation, there is no compelling reason for baryon number to be conserved. In fact, most modern particle physics theories, like GUT models and Supersymmetry, allow for baryon number violation. Nevertheless, until particle physics experimental data provides confirmation of these ideas, the observed lack of antimatter in our part of the Universe will be the strongest evidence for baryon number violation [5].

An exact CP symmetry would imply that the branching ratios for the decays of any objects into matter would be the same as for decays into antimatter, preventing any net gain for matter over antimatter even if baryon number were not conserved².

In standard baryogenesis scenarios, such as those evolving from GUTs, whether matter or antimatter is created in a given region of the Universe in the early Big Bang depends on the sign of the CP violation parameter. If CP violation arises from spontaneous symmetry breaking (rather than being built into the Lagrangian function that describes the fundamental particle interactions), then it is possible to form domains of antimatter and domains of matter. If inflation (exponential expansion of the Universe) occurred after the domains appeared, the entire observable Universe would likely be a single domain of one sign (i.e., completely made of matter or antimatter). The discovery of large-scale domains of antimatter would show that somehow domains with both signs occur in our Universe [5]. These regions could inflate to cosmologically significant scales.

The study of the baryon asymmetry of the Universe provides crucial information in attempts to probe beyond the Standard Model of particle physics.

Indirect observations of antimatter can be obtained by studying the energy spectrum of the electromagnetic radiation. A high flux of γ rays could be produced by the $p\bar{p}$ and e^-e^+ annihilations that must abundantly occur near the borders of domains where a substantial quantity of antimatter would be present together with matter or in regions where baryons and antibaryons (as well as leptons and antileptons) would be well mixed [6].

The $p\bar{p}$ annihilation must result in the abundant production of neutral pions, whose decay produces photons extending from several tens of MeV to several hundred MeV. The observed diffused γ -ray energy spectrum does not show any evidence for a bump at these energies, but it allows us to set limits on the quantity of antiprotons in the space around us. These limits can be expressed in terms of the fraction of antiprotons with respect to protons that could be mixed in different volumes: the antiproton content

¹If the baryon asymmetry was created through B-violating decays of a meson (M) into a baryon (B) and a lepton (L): $M \rightarrow B + \bar{L}$, and $M \rightarrow \bar{B} + L$, then in thermal equilibrium one must take into account not only the inverse reactions $B + \bar{L} \rightarrow M$ and $\bar{B} + L \rightarrow M$, but also direct scattering $B + \bar{L} \rightarrow \bar{B} + L$, which effectively reestablishes baryon symmetry.

²An example of CP violation which illustrates the point regarding baryogenesis involves the following two decay modes: (a) $K_L \rightarrow \pi^+ + e^- + \bar{\nu}_e$, (b) $K_L \rightarrow \pi^- + e^+ + \nu_e$. Since CP takes the right side of (a) into the right side of (b), CP conservation would imply equal branching ratios for (a) and (b) if the K_L were a pure eigenstate of CP. That this is not the case is reflected by the observation that (b) proceeds by a fractional amount 0.0033 greater than (a). This is a process that makes an absolute distinction between matter and antimatter.

cannot exceed 10^{-15} of protons in the nebulae of a galaxy, 10^{-10} in the galactic halo, and 10^{-5} in our cluster of galaxies. Considering that the number of clusters of galaxies in the explored Universe can be estimated to exceed 10^8 , one can regard the above values as "local" limits that provide no information about the Universe on large scales.

Direct observation of positrons. High-energy cosmic-ray electrons and positrons are of particular interest because their transport and lifetime in interstellar space are affected by several radiative energy-loss mechanisms that do not affect cosmic-ray nuclei of similar energies. These include synchrotron losses in the galactic magnetic field, bremsstrahlung losses on interstellar matter, and inverse Compton scattering on visible and 2.7 K blackbody photons. Consequently, they can reveal aspects of cosmic-ray source distribution and cosmic-ray transport in the galaxy that are not evident from studies of nuclei alone. About 1 per cent of cosmic rays by number are electrons and positrons together. It is just unclear why cosmic rays include approximately 100 times more nuclei than electrons and positrons.

The fraction of positrons is an important diagnostic for the origin of the electron component. If all electrons and positrons were of secondary origin, produced along with the diffuse γ radiation from pion decay ($\pi^\pm \rightarrow e^\pm$), then the positron fraction would be 1/2. Current positron data come from balloon-borne magnetic spectrometers; these studies are complicated by the background of positrons produced by cosmic-ray interactions in the upper atmosphere. The typical ratio expected from the model considerations is about 5–10%, if all primary electrons have negative charge.

Cosmic-ray electrons and positrons have enormous potential for revealing new information about cosmic rays in the galaxy, but this potential has often been frustrated by a combination of factors, including uncertainties in the atmospheric background and possible heliospheric effects, as well as the inherent difficulty of the measurements. Most of the difficulties will be overcome by the Alpha Magnetic Spectrometer in space that could separate electrons and positrons over a broad energy interval with good statistical accuracy. Therefore, precise determination of this flux at very high energies will furnish fundamental information about the dynamics of the galaxy.

Direct observation of antiprotons. Antiprotons are a unique tracer of cosmic-ray origin. Like other secondary species, they are produced by interactions of cosmic rays, either during propagation or in the material near their sources. The basic reaction for producing antiprotons in high-energy collisions, $p + p \rightarrow p + p + \bar{p} + p$, requires an incident proton with a kinetic energy of about 6 GeV or more. The ratio between this secondary antiproton flux and the proton flux can be reasonably well evaluated by using some model for the propagation of cosmic rays in the galaxy. The \bar{p}/p ratio is very low at 100 MeV and increases with the energy, reaching the maximum $\bar{p}/p \simeq 10^{-4}$ at about 10 GeV. Cosmic-ray antiprotons differ from other secondary nuclei in several important ways. They are produced mainly by collision of protons rather than nuclei. The energy of the parent particle is much higher than that of the secondary antiproton, and the production cross section for antiprotons is strongly energy dependent because of the large mass that must be produced. Unlike positrons, antiprotons do not suffer significant radiative losses.

If the flux of cosmic-ray antiprotons is confirmed to be greater than expected from secondary production by cosmic rays colliding with the interstellar gas, it may provide evidence for one of several possibilities. It may be that many cosmic-ray protons have

traversed more material than heavier elements such as C, N, and O because there are additional sources of cosmic-ray protons such as supernova remnants surrounded by shells of matter. There may also be more exotic sources of antiprotons such as the decay of massive particles left over from the Big Bang. Finally, there is the possibility of "primary" cosmic-ray antiprotons originating in condensed regions of antimatter beyond our galaxy. Precise measurements of antiprotons over the widest possible energy range are needed to address these possibilities.

Until now, all data have been obtained in balloon experiments, so that an important background due to antiprotons produced by cosmic-ray interactions with the residual atmosphere overlying the apparatus must be subtracted, which increases uncertainties. Until now, the highest reached energy is near 15 GeV, where the differences between the predictions of various models are not decisive. Furthermore, experimental results at the highest energies are somewhat contradictory, so that further refinements and enlargement of statistics must be provided. To obtain clearer results, with much higher statistics, and reach much higher energies, the AMS project measurements outside the terrestrial atmosphere are just in order.

Search for antinuclei. A definitive answer to the question of whether antimatter exists on astronomical scales can come from the possible discovery of an antinuclear component in cosmic rays. The possibility that an antinucleus could be secondarily produced by energetic protons is very remote (the rate of secondary production for anti- ${}^3\text{He}$ is less than 10^{-11} times the rate for antiproton production), so that a detected antinucleus, if any, cannot be considered to be of secondary origin. Therefore, this is a measurement cleaned from any physical background. Detection of such antinuclei would imply the existence of antimatter domains within 100 Mpc (from which antimatter cosmic rays are able to escape) as well as the sufficiently weak wind from our galaxy so that antinuclei can get in.

If we assume that antimatter behaves, on the astronomical scale, in the same way as matter (the space at large were to contain equal numbers of galaxies and antigalaxies), antimatter cosmic rays might be found at a level of one in every 10^5 or 10^6 helium nuclei. Therefore antihelium nuclei must be the most abundant (about 10% of the dominating antiprotons) and antihelium is the easiest antinucleus to be detected [6]. However, the meaning of antihelium detection would not be unique, because antihelium could also be of primordial origin, synthesized just after the Big Bang, and not in the interior of an antistar. In general, the existence of only one heavy ($Z \geq 3$) antinucleus implies that antimatter exists on the astronomical scale, at least at a level of galaxy clusters. Until now, the limits on the existence of antinuclei have been commonly expressed in terms of the $\overline{\text{He}}/\text{He}$ ratio because of the low sensitivity that could be reached for similar ratios between other nuclei. Direct measurements of antimatter fluxes were made so far in the balloon experiments - BESS, CAPRICE, HEAT, WiZard etc. [7]. Recently the BESS collaboration has reported the upper limit $\overline{\text{He}}/\text{He} = 8 \times 10^{-6}$ [8].

The present experimental situation can be summarized as follows. 1) The positron flux is dominated by secondarily produced positrons at all energies. 2) The antiproton flux is dominated by secondarily produced antiprotons up to about 5 GeV. 3) The antiproton flux data at higher energies are in conflict and do not yield firm indications. 4) For the flux of antinuclei, we have obtained only upper limits.

The AMS collaboration [9] will carry out the most sensitive search ever done (im-

proving the existing sensitivity by a factor of 10^4 or 10^5) for cosmic-ray nuclei (helium, carbon, oxygen) made of antimatter, the presence of which would prove the existence either of large-scale primordial regions made of antimatter (if antihelium is discovered), or of stars made of antimatter (if antinuclei with atomic number greater than that of helium are discovered).

The current levels achieved are not sensitive enough to test the existence of super-clusters of galaxies of the antimatter; the sensitivity of AMS is 10^3 times higher than this prediction based on the matter-antimatter symmetric Universe.

1.2 Dark matter

Another cosmic-ray window on cosmology relates to dark matter, which probably constitutes more than 90 per cent of the mass of the Universe. The largest part of this dark matter must be non-baryonic particles which are unknown in the Standard Model of particle physics, most likely weakly interacting massive particles (WIMP). Annihilation of pairs of such particles in the halo of our galaxy could produce antiprotons, positrons, and photons, which could be detected by cosmic-ray experiments.

The most promising photon signal would be from monochromatic γ -ray lines, which could result from WIMP, χ , annihilation like $\chi\bar{\chi} \rightarrow \gamma\gamma$. A successful search would require that the annihilation cross section be large, that there be some concentration of WIMPs, and that the backgrounds, currently not that well known, be favorable. Measurements over the range from 1 GeV to 1 TeV will require a combination of techniques.

Antiprotons could provide a more likely detection signal, especially those of very low energy (< 1 GeV), where the background of secondary antiprotons from interactions of cosmic rays in the interstellar gas is suppressed by kinematics. Even if an excess of antiprotons is observed, however, this by itself will not be direct evidence for dark matter, since there is still too much uncertainty about antiproton production in cosmic-ray propagation. Anyway, together with other data from accelerator experiments this observation would bring strong limitations for modern extensions of the Standard Model.

Of the many dark matter WIMP candidates, perhaps the best motivated and certainly the most theoretically developed is the neutralino, the massive, Majorana-like, weak-interacting, lightest supersymmetric particle (LSP), which is stable within R-parity conservation [10]. Supersymmetry is the theoretical favorite for an extension of the Standard Model, and there are many planned and already running direct, indirect and accelerator searches for such neutralinos.

Despite the fact that more than 90% of the Universe is believed to be non-baryonic the hypothesis that the dark matter of the Universe includes a significant component in the form of primordial black holes is not verified or eliminated yet. The smallest black holes would have evaporated by now, and those evaporating in the present epoch would be about 10^{15} g. The existence of primordial black holes can be inferred from the cosmic background gamma radiation or the cosmic background of neutrinos, which would have accumulated from evaporation of the smaller black holes. However, this radiation could also be due to other causes so that at best an upper limit to the density can be deduced. The best possibility of direct detection comes from the observation of gamma radiation in the final phases of black hole evaporation (Hawking radiation).

In this case the duration of the bursts is a fraction of a second, with the precise decay scenario and time constant heavily dependent on the particle physics model assumed. The final stages of evaporation are sensitive to physics up to the Planck scale and could hold important clues to the coupling of gravity and quantum theory.

The second main goal of the AMS project is to search for dark matter by high statistics precision measurements of \bar{p} , e^+ and γ spectra. These measurements will allow direct searches for various annihilation and decay products of WIMP's in the galactic halo. For example, the accuracy of the AMS measurement of the e^+/e^- spectrum will allow the existence of a heavy neutralino ($m_{\tilde{\chi}} \sim 100$ GeV) to be tested. Also, the measurement of the γ spectrum will test the existence of neutralinos in the case of R-parity violating SUSY models, etc.

1.3 Cosmic Rays

Cosmic rays provide the only direct sample of matter from distant regions of space. To understand the origin of these particles it is necessary to relate the cosmic-ray energy spectrum and composition observed near the Earth to those at the sources. The relative abundances of the elements in the cosmic radiation and their energy spectra contain a record of the nucleosynthetic processes that created this material in stars, of the processes that accelerated some nuclei to cosmic-ray energies, and of their subsequent interactions with matter and fields in interstellar space. By comparing the abundances of secondary and primary cosmic-ray species, and taking into account the probability of producing the secondary species in collisions with the interstellar gas, it has been possible to infer the mean amount of matter traversed by primary cosmic rays during their lifetime.

The transport of cosmic rays from the disk to the halo may be largely controlled by a "galactic wind" (analogous to the solar wind) that convects gas, embedded magnetic fields, and cosmic rays out from the disk. The existence of such a wind would have significant effects on the age distribution and composition of cosmic rays, as diffusion and convection compete. For stable nuclides, the age distribution is entirely determined by the properties of this diffusing and convecting medium.

In the Universe, most of the elements heavier than helium are believed to be produced in stars more massive than the Sun, where lighter elements under intense gravitational pressure and high temperature are able to fuse to make heavier nuclei. A very massive star near the end of its lifetime has an onion-like structure, with the heaviest and most stable elements, such as iron, at its core and progressively lighter elements in the outer layers. Once its nuclear fuel is exhausted, the core collapses to a neutron star or black hole, and a supernova explosion ensues. The shock waves from the collapse heat the outer layers of the star, causing a brief, explosive episode during which further nucleosynthesis occurs. An amount of material greater than the mass of the Sun is injected into the Galaxy and contributes to its chemical evolution.

The most detailed and precise information obtained from the studies of the composition of the nuclear component of galactic cosmic rays has come from measurements of isotopic composition at low energies. In addition to allowing determination of the lifetime of cosmic rays through the measurement of ^{10}Be , cosmic-ray isotope studies have provided evidence that the cosmic-ray material has had a different history of nucleosynthesis than the typical material in our solar system.

One of the main goals of the AMS project consists in the high statistics astrophysical studies of D, ^3He , B, C, ^9Be and ^{10}Be spectra. AMS will measure about 10^9 deuterium events, thus reducing the current uncertainty on D/p by a factor of 10^3 . AMS will be able to separate ^3He from ^4He , strongly reducing the existing uncertainties. The ratio B/C, which constrains the parameters regulating the outflowing galactic wind, can be measured by AMS with high statistics. The ratio $^{10}\text{Be}/^9\text{Be}$ determines the cosmic ray confinement time. At present, a dozen ^{10}Be events have been detected during more than fourteen years of observations, and the cosmic ray galactic confinement time is currently known within a large uncertainty ($\sim 40\%$). With AMS it will be possible to detect tens of ^{10}Be per day, thus dramatically reducing the error on cosmic ray confinement time.

The table summarizes the main physics capabilities of AMS [9].

Table 1: Physics capabilities of AMS after three years on ISSA

Elements	Expected Yield/sensitivity	Now	Physics
e^+ \bar{p} γ	10^9 $5 \cdot 10^5$	$\sim 10^3$ ~ 30	Dark Matter SUSY models R-parity violation
$\bar{\text{He}}/\text{He}$ $\bar{\text{C}}/\text{C}$	10^{-9} 10^{-8}	10^{-5} 10^{-4}	Antimatter CP violation in GUT, EW. etc
D, H_2 $^3\text{He}/^4\text{He}$ $^{10}\text{Be}/^9\text{Be}$	10^9 10^9 2%		Astrophysics Cosmic rays propagation Cosmic rays confinement

2 TCAL peculiarity

A few advantages can be obtained in AMS with TCAL of high longitudinal and transverse granularity:

- In the energy region of a few GeV per nucleon, where the maxima of all experimentally measured nucleon and nucleus spectra are observed, a sufficiently deep TCAL can provide identification of helium or antihelium events in addition to the AMS tracker.
- An important problem in the antimatter search is separation of electromagnetic showers (electrons and positrons) from hadronic showers (antiprotons and protons). Monte Carlo simulation of TCAL properties showed that such separation at the level of 10^{-4} in the 5–50 GeV energy region is possible. TCAL rejection power depends only slightly on the energy of incident particles.

- The primordial gamma ray spectrum measurements in tens-GeV region are necessary for the study of many astrophysical problems including the problem of existence and composition of dark matter. To this end a thin 0.3 radiation length tungsten convertor is supposed to be placed in front of the tracker for measurements of converted electrons and positrons. A disadvantage of this method is the additional material which would be probably the main source of background events in the antimatter search. The fine-granulated TCAL can measure high energy photons with good angular and energy resolution without any generation of additional backgrounds events.
- In high precision experiments, as the AMS project is supposed to be, a proper understanding of the background is crucial. Such background events will be the albedo events due to ordinary high energy cosmic ray interactions in the upper layers of the Earth's atmosphere [11]. Secondary charged particle propagation is very complicated due to the geomagnetic field (0.5 gauss) in the region up to tens of GeV. A simple picture where albedo particles enter the AMS from below is valid only at the high energy edge of the particle spectra but not in a few-GeV region containing the main bulk of particles. Albedo gammas, neutrons and antineutrons are produced in the same reactions as the charged particles and can reach the AMS detector, but their trajectories are not changed by the geomagnetic field. The unique TCAL ability to measure neutral gammas, neutrons and antineutrons will be useful for the proper understanding and correct interpretation of the charged particle and antiparticle fluxes.
- Even if one antinuclear candidate is found in the AMS detector, it will be considered as the most significant antimatter signal. Certainly, such an event should be carefully checked to exclude any chance of misinterpretation. In the off-line analysis the fine granular TCAL, as an additional tracker with a few mm spatial resolution, provides detailed information about an event, in particular, for antinuclear events which would have distinct signatures.

3 General layout of TCAL

The track calorimeter (TCAL) consists of 30–50 layers of thin and long (≈ 80 cm) scintillator strips which are perpendicular to the z axis (AMS axis) and alternatively directed in the x and y axes in adjacent layers. The transverse size of a scintillator strip is about 7.5×7.5 mm². The passive material, 1–3 mm thick, of uranium, lead or tungsten is situated between the layers. With such a device it is possible to get a fast calorimeter signal for trigger purposes together with rather finely granulated images of individual tracks of charged particles. The images can be used for detailed off-line investigation of an event including the type of the initial particle or nucleus. The scintillation light signals from separate counters will be detected at their ends with PMTs.

Fine granularity of TCAL provides good measurement of a shower shape and, as shown below, allows separation of hadron and electromagnetic particles in the wide energy interval. High-precision TCAL measurements of the energy and direction of gammas in the region of tens of GeV are important for the dark matter search.

3.1 The calorimeter response for nuclei and antinuclei

For the calorimeter geometry described, the Monte Carlo study was performed by means of the general purpose simulation program GEANT3.21 [12]. For simplicity, the nucleus-nucleus interaction inside the calorimeter was considered in the one-nucleon approximation, i.e. assuming that only one nucleon of the incident nucleus interacts with the target nucleus and the other nuclei are spectators.

The preliminary results of the investigation of the Scintillator-Iron calorimeter response are as follows. As an example, the dependence of the calorimeter response on the value of energy/nucleon ratio for He and $\bar{\text{He}}$ is presented in Fig. 1. The total energy loss, E_{loss} , of all charged particles inside the sensitive volume was taken for the calorimeter response. The Monte Carlo simulation of 100-layer Sc-Iron TCAL shows the clear difference in the calorimeter response for He and $\bar{\text{He}}$ in the energy/nucleon region up to a few GeV where the TOF system can provide measurement of the momenta of incoming nuclei.

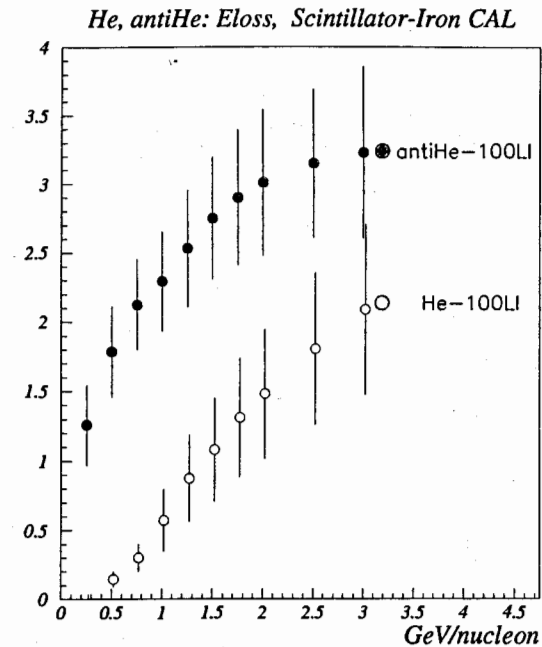


Figure 1: Momentum dependence of the energy loss in the iron-scintillator calorimeter for helium and antihelium. "Errors" correspond to the resolution values.

As was mentioned above, the maxima of the ordinary nucleus spectra are in the 1-GeV/ n region and there are no convincing reasons to expect a different spectrum for antinuclei. The probability of the 1-GeV/ n He to produce a response like that of the antihelium is rather small ($\sim 10^{-4}$). Therefore the search for antinuclei is possible in this region with the TCAL detector alone.

3.2 Measurements of high energy gamma rays

The measurements of energy and directions of gammas at tens of GeV are necessary for the dark matter search as indicated before. The high granularity of TCAL with a depth about 10 radiation lengths meets this requirement. The TCAL, consisting of 30 U(2 mm)–Sc(7.5 mm) layers, has the energy resolution $\sigma/E = 6\%/\sqrt{(E)} + 6\%$, as one can conclude from the Monte Carlo results presented in Table 2.

Table 2: 30-layer U(2 mm)–Sc(7.5 mm) TCAL energy resolution for incoming electrons.

E , GeV	E_{loss} , GeV	σ	N_{events}
5.0	0.602	0.053	50000
10.0	1.204	0.095	25000
30.0	3.598	0.266	30000
50.0	5.976	0.441	25000

The angular resolution of such a calorimeter for the tens-GeV gammas is about 1° ; however, more precise simulation and experimental studies are necessary to obtain more accurate estimation of the value.

4 TCAL for separation of hadronic and electromagnetic showers

At the energy above 5 GeV, the electron-hadron separation in AMS with the existing TOF and aerogel Cherenkov detectors is not efficient enough. Therefore it is particularly interesting to compare the electron and antiproton shower parameters in TCAL to study its selection capability.

A few parameters for shower description have been used in the TCAL simulation to study its selectivity properties, namely, total energy deposition in TCAL, E_{loss} , average transverse x - and y -size of a shower:

$$\langle x \rangle = \frac{\sum_i |x_i| E_{\text{loss}}^i}{\sum_i E_{\text{loss}}^i}, \quad \langle y \rangle = \frac{\sum_i |y_i| E_{\text{loss}}^i}{\sum_i E_{\text{loss}}^i} \quad (1)$$

where x_i , y_i are the distances between x - or y -directed scintillator strips and the shower axis. The summation is over all hit counters.

Two additional parameters χ_e^2 and D_{L3} were defined in reference to the electromagnetic longitudinal shower profile:

$$\chi_e^2 = \sum_{i=1}^{N_L} \left(\frac{E_i^r - E_{\text{loss}}^i}{\sigma_i^r} \right)^2, \quad (2)$$

$$D_{L3} = \frac{\sum_{i=1}^{N_L} \left(\frac{E_i^r - E_{\text{loss}}^i}{E_i^r + E_{\text{loss}}^i} \right)^2 (E_i^r + E_{\text{loss}}^i)}{\sum_i (E_i^r + E_{\text{loss}}^i)} \quad (3)$$

where E_i^r , E_{loss}^i are the reference and measured responses in the i th TCAL layer, N_L is the total number of TCAL layers. The parameter D_{L3} was successfully used for the calorimetric analysis by the L3 experiment at LEP. The χ_e^2 and D_{L3} parameters are based on the same longitudinal shower profile and are rather strongly correlated (see below).

The reference E_i^r distributions are defined for the given momentum of the incoming positron and are presented in Fig. 2 for $\vec{p} = (p_x, p_y, p_z) = (0, 0.5, 5)$ GeV/c and $\vec{p} = (0, 5, 50)$ GeV/c. Distributions of these shower parameters for 10-GeV protons and positrons are presented in Figs. 3 and 4.

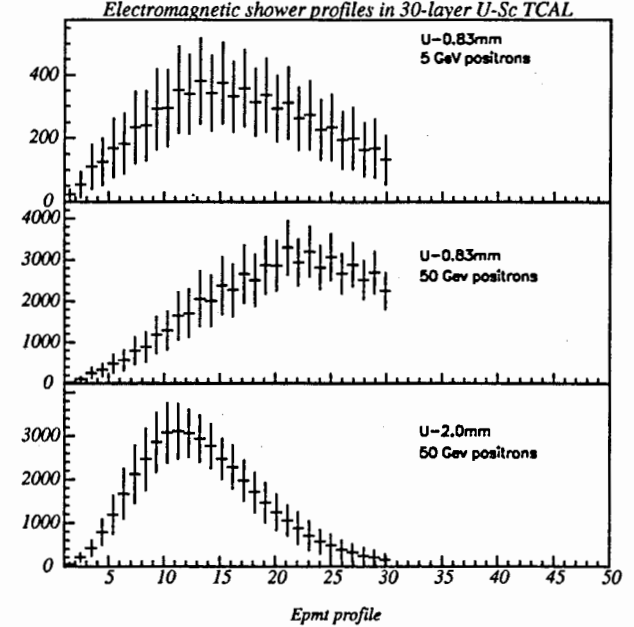


Figure 2: Longitudinal shower profiles in TCAL for $\vec{p}_e(0, 0.5, 5)$ GeV/c and $\vec{p}_e(0, 5, 50)$ GeV/c positrons. Epmt is the total PMT response per layer (in number of photoelectrons).

The relative efficiency of these parameters in the selection between hadronic and electromagnetic showers can be evaluated by the corresponding resolution values for these variables. Table 3 presents the efficiencies for the TCAL of 30 layers and 7.5×7.5 mm² strips.

These figures were obtained for incoming electrons or positrons with momenta around 10 GeV/c. The better the resolution value, the more efficient the parameter for the selection. One can see that E_{loss} , $\langle x \rangle$, $\langle y \rangle$ are the most sensitive parameters in the selection between hadron and electron showers. In the TCAL simulation the AMS momentum resolution was taken to be equal to 7% in the interval 2–20 GeV/c and was linearly increased to 100% at 500 GeV/c. The events induced by incoming hadrons fall into two subsets with different resolution characteristics: hadron showers and punch-through hadrons.

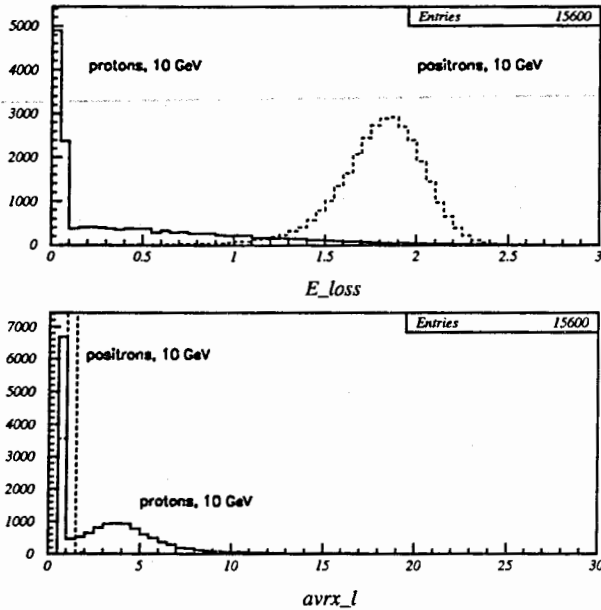


Figure 3: TCAL response for 10-GeV positrons and protons. Visible energy loss distribution in GeV is presented in the upper panel. The distribution of the weighted x -projection of transverse size in cm is given in the lower panel.

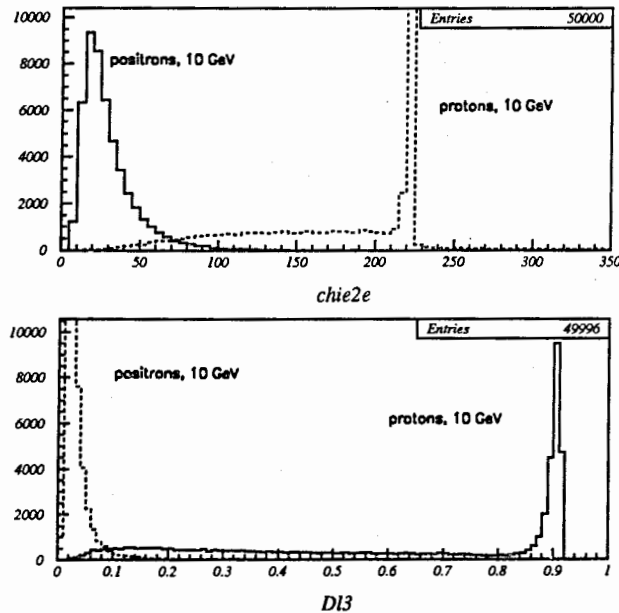


Figure 4: Characteristics of the shower for 10-GeV positrons and protons based on the comparison with the reference electromagnetic shower in TCAL. The explanations are in the text.

Table 3: Rejection power of different cut parameters for the TCAL with $7.5 \times 7.5 \text{ mm}^2$ scintillator strips. The first two lines correspond to TCALs of the same weight.

Absorber	N_{layers}	Weight, kg	$\frac{\sigma}{E_{\text{loss}}}$	$\frac{\sigma}{\langle x \rangle}$	$\frac{\sigma}{\langle y \rangle}$	$\frac{\sigma}{x^2}$	$\frac{\sigma}{D_{L3}}$	\bar{p} , GeV
U, 0.83 mm	30	450	0.14	0.16	0.12	0.60	1.00	0,1,10
Fe, 2.0 mm	30	450	0.34	0.24	0.17	0.83	1.10	0,1,10
U, 2.0 mm	30	880	0.077	0.15	0.12	1.25	0.74	0,1,10
U, 3.0 mm	30	1240	0.084	0.17	0.17	-	-	0,0,10
U, 3.0 mm	50	2070	0.089	0.13	0.13	-	-	0,0,10
Fe, 2.0 mm	100	1500	0.077	0.11	0.11	-	-	0,0,10

4.1 Properties of electromagnetic and hadronic showers in TCAL

To investigate the discrimination power of TCAL, a large number of electron and antiproton showers were simulated. The analysis shows that electron showers develop "earlier" and are narrower than antiproton showers. How often can an electron mimic an antiproton and vice versa when suitable cuts are applied which do not decrease very much the efficiency for antiproton collection?

The answer to this question can be found from Table 4 where the suppression of the electron or proton showers is presented for the 30-layer TCAL. Electromagnetic shower suppression was achieved by the following requirement: the transverse average $\langle x \rangle$ -size should be less than 0.5 cm (punch-through hadron selection) or greater than 0.8–1.0 cm (hadron shower selection). The same cut is simultaneously applied to the average $\langle y \rangle$ -size.

Table 4: Separation between electron and antiproton showers at different energies for the 30-layer TCAL of $7.5 \times 7.5 \text{ mm}^2$ scintillators.

Absorber thickness	Momenta, GeV/c	# Simulated events	e^- -suppression		p^- -suppression	
			supp $_e \cdot 10^4$	eff $_p$	supp $_p \cdot 10^4$	eff $_e$
U, 2 mm	0,0,5	50000	1.0	0.88	0.4	0.88
U, 2 mm	0,0,10	25000	0.4	0.92	1.6	0.97
U, 2 mm	0,0,20	50000	0.2	0.91	0.8	0.95
U, 2 mm	0,0,30	30000	0.3	0.93	1.3	0.97
U, 2 mm	0,0,50	25000	1.2	0.95	1.6	0.99
U, 2 mm	0,1,10	60000	0.0	0.97	0.0	0.99
U, 0.83 mm	0,1,10	50000	0.8	0.97	2.0	0.93
Fe, 2.0 mm	0,1,10	40000	2.5	0.85	1.8	0.91

For hadronic shower suppression other cuts were used: $\langle x \rangle$, $\langle y \rangle$ should be less than 0.8–0.9 cm and the total energy loss in the first 10 layers should be greater than 0.140–0.350 GeV depending on the energy of the incoming particle. For the 5-GeV energy

an additional cut in the total energy response was also used. The last three lines in Table 4 present the results obtained for the tracks inclined to the x - y plane (the cuts used are those presented in Figs. 5–10). The last two lines correspond to the U-Sc and Iron-Sc TCALs of the same weight with about $8.3X_0$ and $4X_0$ radiation lengths respectively. In all cases the TCAL electron-hadron selectivity is at the same level of 10^{-4} irrespective of the incoming particle energy. The selectivity can be improved by more sophisticated cuts.

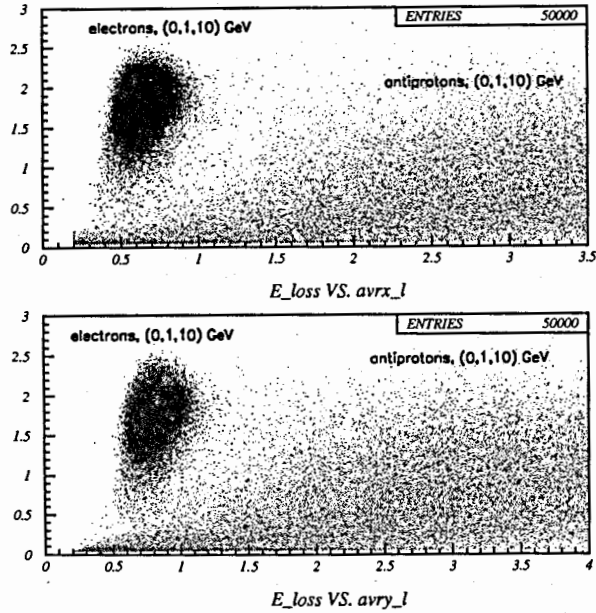


Figure 5: E_{loss} versus $\langle x \rangle$ (above) and E_{loss} versus $\langle y \rangle$ (below) for electron and antiproton showers with $\vec{p} = (0, 1, 10)$ GeV/ c in the track calorimeter of 30 Sc-U layers.

A higher classification power may be achieved with the neural net approach. Neural net classifiers would exploit the knowledge of the joint probability distribution of various features of registered showers. Under certain conditions the neural net classifiers realize the asymptotically optimal Bayesian decision.

It is quite probable that the existing simulation procedure is not valid at this level of accuracy and the results should be confirmed experimentally. The relevant SPACAL [13] experimental data exists and shows that such a separation level may be reached. Therefore, there are no physical obstacles for TCAL to reach the same accuracy in separation.

4.2 TCAL as a tracking device

The proposed calorimeter has the fine structure and may be considered as a rather good tracking device. All tracking information of the selected events will be initially filtered

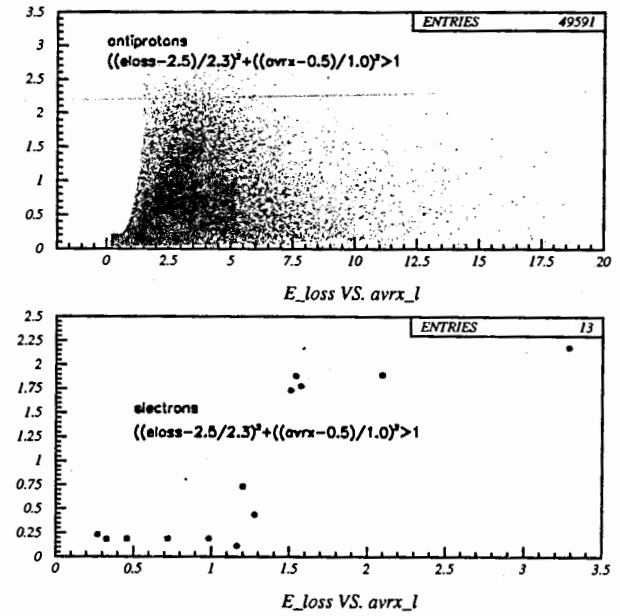


Figure 6: Antiproton selection with a 2-dimensional $E_{\text{loss}}-\langle x \rangle$ cut. The $E_{\text{loss}}-\langle y \rangle$ cut gives similar results.

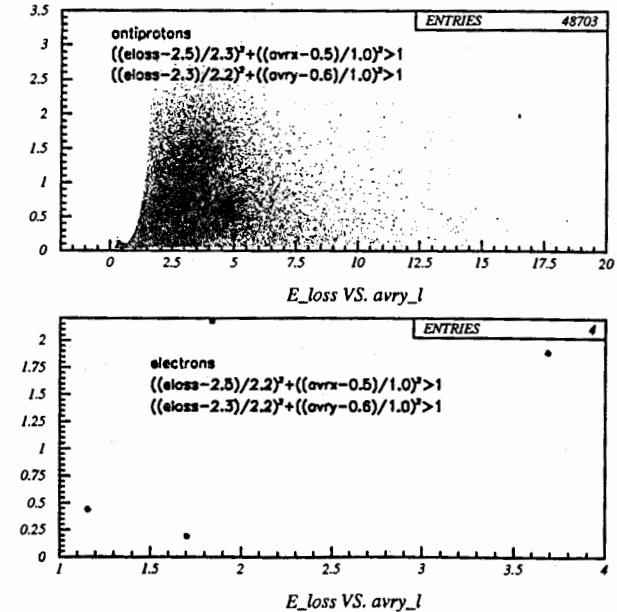


Figure 7: Antiproton selection with the simultaneous $E_{\text{loss}}-\langle x \rangle$ and $E_{\text{loss}}-\langle y \rangle$ cuts.

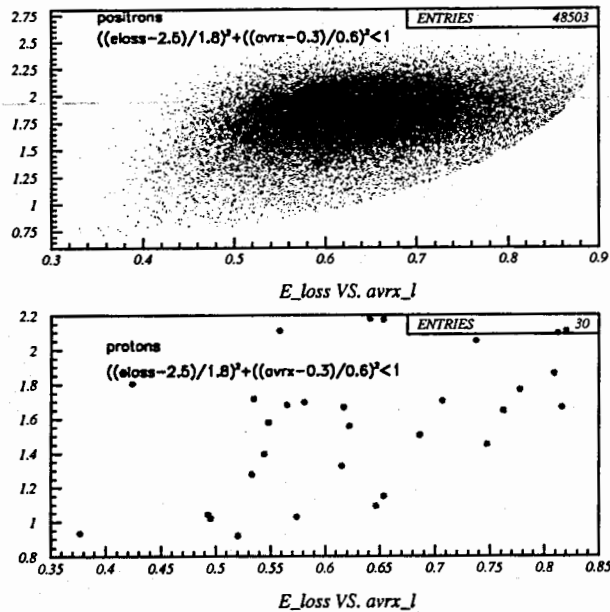


Figure 8: Positron selection with a 2-dimensional $E_{\text{loss}}-\langle x \rangle$ cut. Similar result was obtained with the $E_{\text{loss}}-\langle y \rangle$ cut.

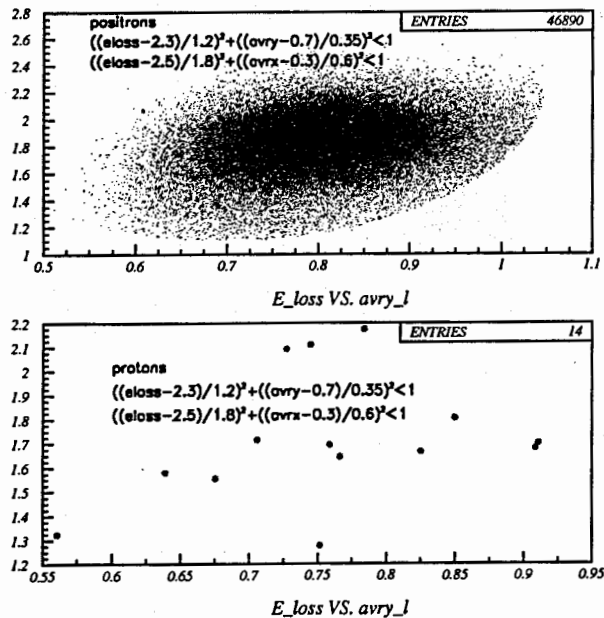


Figure 9: Positron selection with the simultaneous $E_{\text{loss}}-\langle x \rangle$ and $E_{\text{loss}}-\langle y \rangle$ cuts.

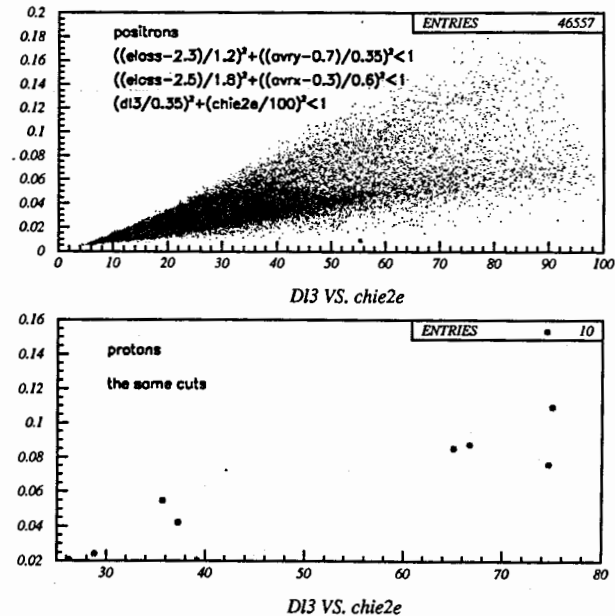


Figure 10: Additional selection of positrons with the 2-dimensional cuts based on the parameters calculated by comparison with the reference electromagnetic shower. More explanation is in the text. Correlation between the shower parameters D_{L3} and χ_e^2 is clearly seen.

by the on-board computers, compressed and stored for transmitting to the Earth for subsequent off-line analysis.

The tracking potential of the calorimeter can be seen from Fig. 11 where the xz and yz projections of the 1-GeV/ n antideuteron interaction inside the calorimeter are shown, as the interaction is registered by the corresponding x and y scintillator strips of the calorimeter. Two different space vertices relevant to the interaction of the antiproton and antineutron are clearly seen. In approximately 50% of the antideuteron interactions one of the antinucleons would play the role of a spectator [14], and in 20% of such events two separate vertices would be visible. It is important to note that this tracking capacity of the calorimeter is practically independent of the initial energy.

The use of the tracking property of the calorimeter might give a possibility of associating secondary tracks, which could appear in interactions of different (anti)nucleons from incoming (anti)nuclei, and the corresponding energy or hit responses. Such off-line analysis could help to identify initial nucleus and antinucleus events even at high energies (in the cases when most secondary tracks of primary vertices are visible inside the calorimeter).

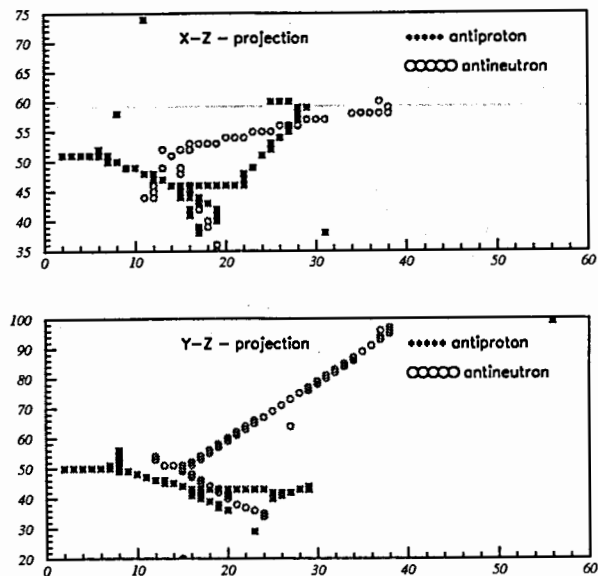


Figure 11: Image of the yz - and xz -projections of the 1 GeV/ n antideuteron interaction inside the uranium-scintillator tracking calorimeter.

5 Preliminary R&D

R&D study with cosmic muons has already started at JINR. The aim of the investigation is to check the detector operation and to fix some parameters for the Monte Carlo simulation of TCAL. The results of this investigation are presented in Table 5 and Fig. 12.

Table 5: R&D results with TCAL Sc-strips of different transverse sizes and Hamamatsu R5900 PMTs. The second number in the first column is the thickness of the scintillator along the path of incoming cosmic muons. The study was performed without optical grease inside the fiber groove.

Sc-size, mm ²	Sc-area	ph.e/MIP
10 × 10	100	7.9
10 × 7	70	8.1
7 × 10	70	10.4
7 × 5	35	8.1
5 × 5	25	9.1

A few polystyrene scintillator strips 80 cm long with different transverse sizes were manufactured. A WLS fiber (Kuraray Y11, 1.5 m long and 1 mm in diameter) drawn

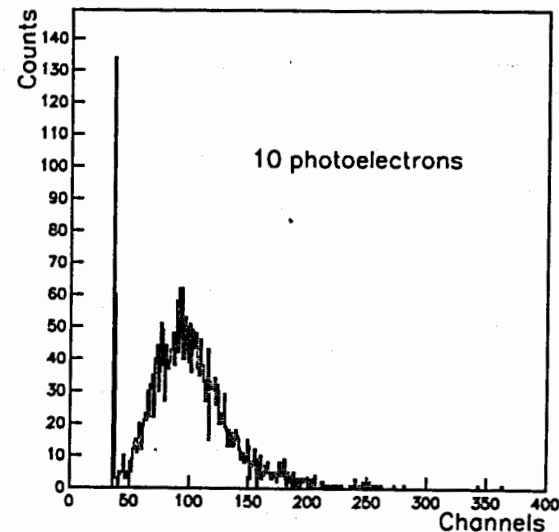


Figure 12: Cosmic muon study of a $5 \times 5 \times 800$ mm³ polystyrene scintillator strip with a 1.2×1.2 mm² groove without optical grease inside for the WLS fiber (Kuraray Y11, 1.5 m long, 1 mm in diameter, mirrored end). The distribution of ADC signals for the 1.3-m distance between the PMT cathode and μ -tracks.

in a groove (without the optical grease inside) along one of the strip side was used for light collection. Hamamatsu R5900 PMTs under HV 900 volts were used as light receivers. These results are in good agreement with the published D0 results [15].

Depending on the quality of the optical contact between the scintillator strip and the WLS fiber, a clear MIP signal was obtained with about 7–12 photoelectrons on the PMT cathode. Thus, the "scintillator + fiber" combination may serve as a good basis for the use in TCAL for the AMS experiment.

The first prototype TCAL planes were fabricated and tested with cosmic muons and radioactive sources. The planes with different designs of strips were scanned perpendicular to the strip orientation axes by a source equipped with a narrow 1-mm collimator. The light from a strip in the plane was collected to PMT by a fiber and the resulting PMT current was measured. In Fig. 13a an example of such measurements is presented. Clear strip signals were obtained and used for the optimization of the TCAL strip and plane design.

The TCAL property to discriminate between electromagnetic and hadron showers is crucially dependent on the accuracy of shower shape measurements. In particular, it is important to know dispersion of measured strip currents. The result is presented in Fig. 13b for the values $(I_s - \langle I \rangle) / \langle I \rangle * 100\%$, where I_s is the measured current of the given strip, $\langle I \rangle$ is the average strip current in the plane. The strip signal dispersion is about 10% and may be improved in the final TCAL detector design.

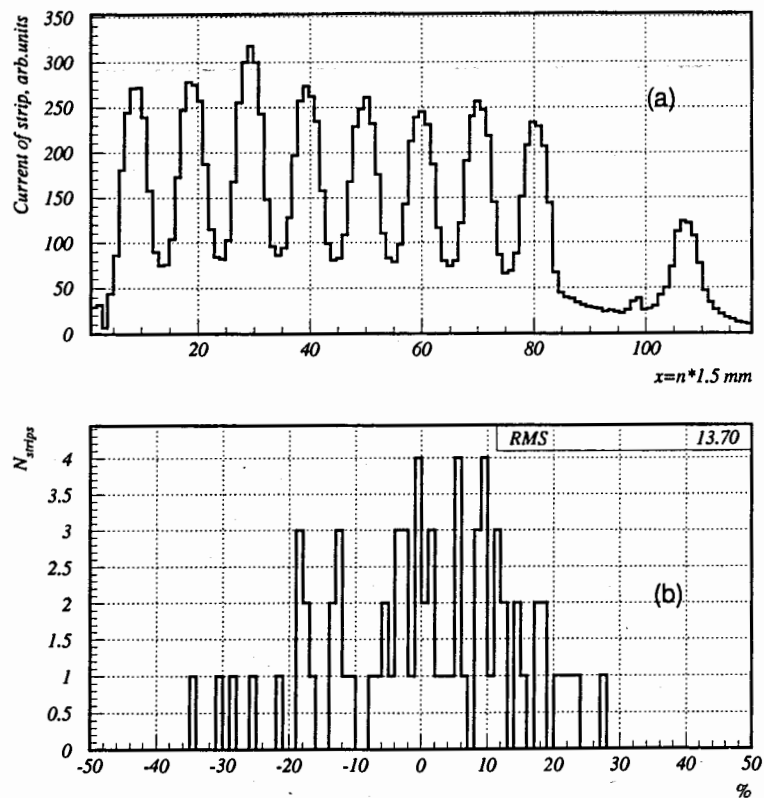


Figure 13: Test results of prototype planes with the radioactive Sr^{90} source. (a) Responses of different strips in the plane, only every second strip was connected to PMT. The separate peak on the right is due to the reference strip out of the plane. (b) Distribution of relative strip signals $(I_s - \langle I \rangle) / \langle I \rangle * 100\%$ for a few planes of different strip designs.

6 The readout system of TCAL

The advantage of the TCAL with scintillator strips is the short decay time ($\sim 10 \text{ ns}$) which is important for hadron-electron shower separation at the level of 10^{-4} due to the possibility of suppressing the pile-up events. Therefore, the readout channel should provide the time resolution at the level of $\sim 10 \text{ ns}$. TCAL should allow one to measure MIP signals and the energy deposit in the maximum of the electromagnetic shower. The dynamic range of the response of TCAL elements from the Monte Carlo estimation is about 1000. The number of amplitude channels of TCAL will be around 4000. For this reason it is supposed to use multianode photomultipliers as light receivers, the readout system similar to the AMS tracker electronics. It is proposed to use front-end amplifiers available from IDE AS. A possible design of the TCAL readout system is presented in Fig. 14.

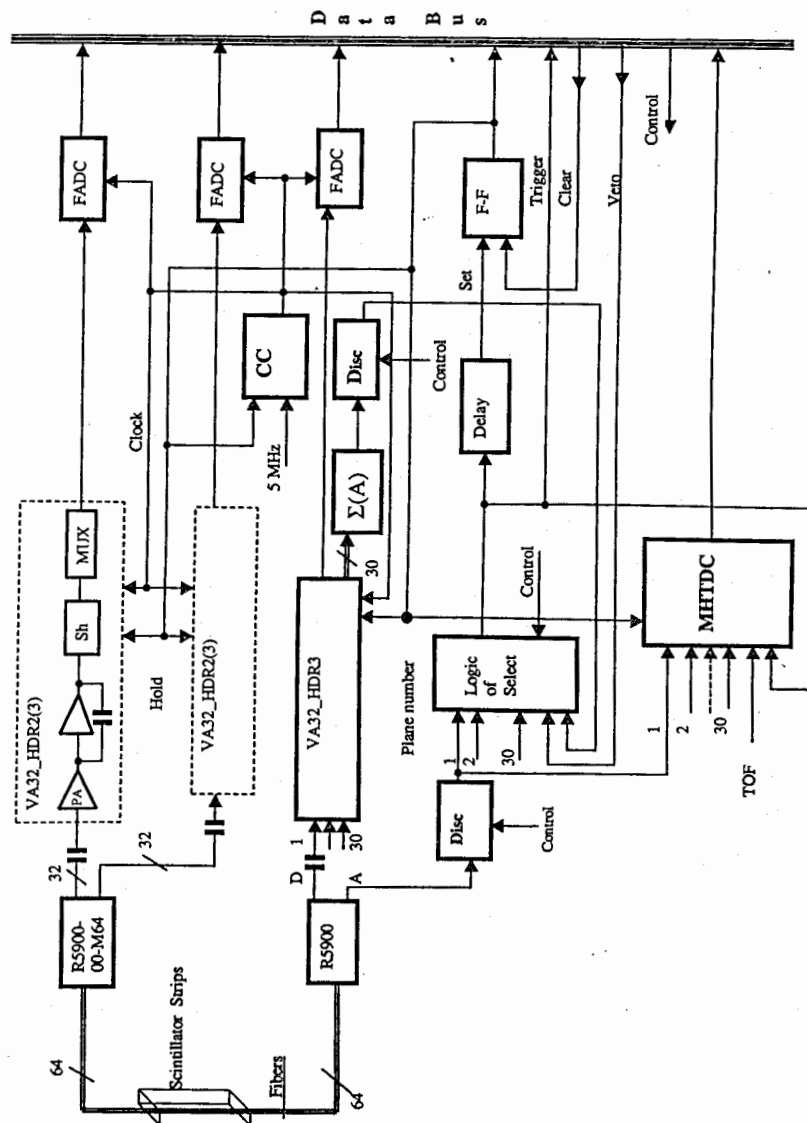


Figure 14: The TCAL readout system

The light from a strip of the calorimeter is collected by two WLS fibers. The first fiber is connected to the multianode HAMAMATSU PMT R5900-00-M64, and the second one is connected to the one-channel PMT. The gain of the multianode PMT is set to be about 10^3 in order to get a PMT linear response up to 0.3 ma. The dynamic range of the PMT output corresponds to about $10^4 - 10^7$ electrons. This range corresponds to the characteristics of the IDE VA32_HDR2 chip (equivalent charge noise $1200e^- + 3.3e^-/pF$, dissipation power 0.2–1.5 mW/ch, peaking-time 1–3 μs , dynamic range ± 230 MIP (1 MIP = $22.400e^- = 3.6 fC$)). It is also possible to use the VA32_HDR3 Viking chip which has the dynamic range ± 550 MIP, but its noise is $4500e^- + 0.7e^-/pF$.

The design of these Viking chips is as follows. Each channel contains a preamplifier with adjustable bias current, a shaper-amplifier with adjustable peaking-time, a sample-and-hold circuit and an analog multiplexer. Each chip contains 32 channels. The readout system consists of two branches.

In the first branch it is offered to use one of the two Viking chips (VA32_HDR2 or VA32_HDR3) for measurement of amplitudes from 64 anodes of the multianode PMT. Thus the output of the analog multiplexer of each circuit is connected to a Flash ADC with a dynamic range equivalent to 14 bits. The second branch of the measuring circuit consists of the peak and time parts.

The measurement of the amplitudes corresponding to the total energy loss in each TCAL layer is carried out with the R5900 penultimate dynodes. Each of these signals is input to one of the VA32_HDR3 channels. The VA32_HDR chips have parallel outputs. The signals from these outputs are passed to the analog adder $\Sigma(A)$ and then to the discriminator with a threshold which may be optimally tuned for the specified energy loss in TCAL. The signal from this discriminator is included into the trigger logic, which may be tuned, for example, for detection of neutral particles. The trigger decision time is about 60–80 ns.

The signals from PMT R5900 anodes are input to the discriminators which allow one to register effectively MIPs. The outputs of these discriminators are connected to the logic circuit inputs and to multihit pipeline TDC inputs (MHTDC) with 1-ns resolution time. Up to 16 successive events can be kept in MHTDC. Besides, the signals from the TOF system and the output of the logic circuit are used as other inputs to MHTDC. MHTDC works in the common stop mode. The output of the logic circuit, delayed by the trigger signal integration time, serves as the MHTDC stop signal (the latter is the output of the flip-flop (F-F)).

The sample-and-hold circuits are switched to the storage mode by the flip-flop signals. At the coincidence with 5 MHz system clock signal the fast AD-transformation of the stored amplitudes by FADC begins. For example, the 'TDRS,K' card with a convertor of the dynamic range equivalent to 14 bits can be used as FADC.

The described circuit realizes the 1st level trigger logic and may use various combinations of signals coming from the TOF system, the tracker, the veto counters and TCAL. The trigger logic may be changed from the Earth.

7 TCAL prototype

TCAL prototype is supposed to be fabricated for the combined beam tests of the detectors, PMTs and electronics at electron-hadron beams of a few GeV.

The main aim of the prototype beam tests is confirmation of the Monte Carlo results concerning the TCAL abilities to separate hadron and electromagnetic showers at the accuracy level of 10^{-4} . The prototype dimensions are determined by the size of hadron showers, which appear in the first layers. Thus, the prototype should have ~ 30 layers with 8–12 strips per layer and, generally, about 300 channels in total. To get test results at the accuracy level 10^{-4} the test beam composition should be known with the same or better precision.

Another aim of the prototype manufacturing and testing is to find a mechanical solution for TCAL which could satisfy space apparatus requirements. RADUGA is the space agency in Dubna which is equipped with all kinds of space test facilities. Complex terrestrial tests (vibrational, overweight, temperature, vacuum, etc) of the TCAL prototype are planned to be performed with the RADUGA standard tools before launching the TCAL apparatus into space.

8 TCAL cost evaluation

Evaluation of the TCAL project (128×32 channels) cost for 1999–2001 is about 1 M\$, which includes equipment, materials, TCAL fabrication and tests in Dubna, TCAL-AMS assembling and joint tests. The 64-channel and one-channel HAMAMATSU PMTs, readout electronic system and expenditures for TCAL-AMS assembling and testing are the main items in the cost evaluation. It would be realistic to apply the 50/50 scheme presently adopted for many CERN-JINR and FNAL-JINR experiments. Participation of the RADUGA space agency in the project gives a chance to get an ISTC grant.

9 Conclusion

In the past forty years, many fundamental discoveries in astrophysics have been made by measuring UV-, X- and γ -rays. There has never been a sensitive magnetic spectrometer in space. AMS will be the first large-acceptance magnetic detector in space. It will allow measurements of the flux of all kinds of cosmic rays with an accuracy of a few orders of magnitude better than before. The essential improvement in sensitivity provided by AMS will allow one to enter a totally new domain in exploring the Unknown.

The JINR contribution — the finely granulated track calorimeter proposed to be added to the AMS detector — would essentially increase the AMS potential in the studies of antimatter, matter and missing matter in the experiments in outer space.

References

- [1] S.C.C.Ting, "Search for Antimatter in Space on ISSA". La Thuile, 1995.
- [2] PAMELA Technical report, RIM-TWO. July 1996.
- [3] P. Papini and P. Spillantini, "Antimatter in the Universe" Physics of Atomic Nuclei, Vol. 59, 1996, p. 1577.
- [4] A.D. Sakharov, Pis'ma Zh.Eksp.Teor.Fiz., 1967, 5, p.24.
- [5] A.D.Dolgov, "Antimatter in different Baryogenesis scenarios", hep-ph/9605280; A. de Rujula, "A matter-antimatter Universe?", astro-ph/9707087.
- [6] K.M.Belotsky, et al., "Antihelium flux signature from antimatter globular cluster in our Galaxy", astro-ph/9807027; M.Yu.Khlopov et al., "Physical origin, evolution, and observational signatures of diffusive antiworld", astro-ph/9810228.
- [7] Golden R.L. et.al., Ap.J., 436 (1994) 769.
Basini G. et.al., Proc XXIV Int. Cosmic Rays Conf., Rome, 3 (1995) 1.
Aversa F. et.al., Proc XXIV Int. Cosmic Rays Conf., Rome, 3 (1995) 9.
Barbiellini G. et.al., Astron. Astrophys., 309 (1996) L15.
Hof M. et.al., Proc XXIV Int. Cosmic Rays Conf., Rome, 3 (1995) 60.
S.W.Barwick et.al., Phys. Rev. Lett. 75, (1995) 390.
S.W.Barwick et.al., Ap.J., 482 (1997) L191.
- [8] J.Ormes, et al. (BESS Coll.) Astrophys. J. 482, L187-L190, 1997.
- [9] R.Battiston, "The Alpha Magnetic Spectrometer (AMS): search for antimatter and dark matter on the International Space Station" hep-ex/9708039.
- [10] G. Jungmann, M. Kamionkowski and K. Griest, Phys. Reports, 1996, 276, p.195.
- [11] S.A.Stephens. Ap. Phys., 6 (1997) 229.
- [12] GEANT Version 3.21. Detector description and simulation tool. CERN, October 1994.
- [13] R.Wigmans, NIM, A315 (1992) 299,
M.Livan, V.Vercesi and R.Wigmans, 1995, CERN Yellow report, 95-02.
- [14] J.Cugnon, Nucl. Phys., A542 (1992) 559.
- [15] M.Adams et.al., 1995, NIM, A366, 263.

Received by Publishing Department
on February 8, 1999.